TEMPERATURE-DEPENDENT PHASE TRANSITION STUDIES OF MULTI-COMPONENT CRYSTALS OF HEXAMETHYLENETETRAMINE AND ISONICOTINAMIDE

CHIA TZE SHYANG

UNIVERSITI SAINS MALAYSIA

2018

TEMPERATURE-DEPENDENT PHASE TRANSITION STUDIES OF MULTI-COMPONENT CRYSTALS OF HEXAMETHYLENETETRAMINE AND ISONICOTINAMIDE

by

CHIA TZE SHYANG

Thesis submitted in fulfillment of the requirements
for the degree of
Doctor of Philosophy

July 2018

ACKNOWLEDGEMENT

I would like to express my deepest appreciation to my principal supervisor, Associate Professor Dr. Quah Ching Kheng and my co-supervisor, Emeritus Professor Dr. Fun Hoong-Kun for their immense knowledge and guidance during the period of my candidature. My sincere thanks go to the academic staffs, postdoctoral research fellows, research officers, lab assistants and lab members whom I met at School of Physics, Universiti Sains Malaysia for their kindness and helps. I like to express my appreciations to Universiti Sains Malaysia and Scientific Equipment Center of Prince of Songkla University for providing the research facilities and services. And many thanks to Professor Angelo Gavezzotti, Professor Mark Spackman and Dr. Thomas Gelbrich for providing the software programs. Also, I am deeply thankful to the Malaysian Government and Universiti Sains Malaysia for the reward of USM Fellowship and the posts of research officer and graduate research assistant. Finally, I would like to thank my family for their endless love and support.

TABLE OF CONTENTS

LIST OF TABLES

LIST OF FIGURES

LIST OF SYMBOLS AND ABBREVIATIONS

a, b, c, α, β, γ	Unit-cell parameters
δ_a, δ_p, δ_d	Dissimilarity parameters
μ	Absorption coefficient calculated from the atomic content of unit-cell, the density and the radiation wavelength
$\Delta\rho_{max}$, $\Delta\rho_{min}$	The largest and the smallest values of final difference electron densities
d_i, d_e	Distances from Hirshfeld surface to the nearest atom interior and exterior, respectively, to the surface
d_{norm}	Normalized contact distance
D_x	Density value calculated from the crystal cell and the contents
E	Normalized structure factor
$E_{coul.}$, $E_{pol.}$, $E_{disp.}$, $E_{rep.}$, $E_{tot.}$	Coulombic, polarization, dispersion (London), repulsion (Pauli) and total energies
E_s	Stabilizing energy (sum of Coulombic, polarization and dispersion energies)
F_o, F_c	Observed and calculated structure factors
$F(000)$	Total number of electrons in a unit-cell
g^+-t-g^-	*Gauche*$^+$-*trans*-*gauche*$^-$ conformation
$Q(C)$, $Q(d,stab)$	Percentages of Coulombic polarization contribution to stabilization and dispersive contribution to total energy
S	Goodness of fit
T_c	Transition temperature
T_{min}, T_{max}	Minimum and maximum transmission factors applied to the diffraction pattern
t+, t–	Fully and non-fully extended all-*trans* conformations
U_{iso}, U_{eq}	Isotropic atomic displacement parameter and equivalent isotropic atomic displacement parameter

w	Weighting scheme
X	Dissimilarity index
Z*, *Z'	Numbers of formula units in a unit-cell and an asymmetric unit
ADP	Atomic displacement parameter
API	Active pharmaceutical ingredient
B3LYP	Becke-three-parameter-Lee-Yang-Parr
CCD	Charge-coupled device
CELL_NOW	A brute-force algorithm for indexing of multi-component non-merohedral and partial merohedral twins
CLP-PIXEL	A model of intermolecular interaction and computer program package
CrystalExplorer	An analysis tool for Hirshfeld surface analysis of crystal structures
DFT	Density functional theory
DSC	Differential scanning calorimetry
FDA	Food and Drug Administration
Gaussian09	A general purpose computational chemistry software package
GRAS	Generally Recognized As Safe
HF	Hartree–Fock
HMTA	Hexamethylenetetramine
IN	Isonicotinamide
IUCr	International Union of Crystallography
IUPAC	International Union of Pure and Applied Chemistry
Mercury	A tool for crystal structure visualisation, exploration and analysis
MP2	Second-order Møller-Plesset perturbation theory
PES	Potential energy surface

PLATON	A versatile crystallographic tool implementing a large variety of standard geometrical calculations, tests, utilities, graphics and several filters
RMSD	Root-mean-square deviation
SADABS	Siemens Area-Detector Absorption
SAINT	SAX Area-detector Integration
SCXRD	Single-crystal X-ray diffraction
SHELXTL	A software package for solving and refining single-crystal X-ray diffraction data sets
SMART	Siemens Molecular Analysis Research Tools
TONTO	A computational chemistry package used in CrystalExplorer for wavefunction calculation and surface generation
TWINABS	Bruker AXS scaling for twinned crystals
vdW	Van der Waals
XL	A command for structure refinement
XPac	A software for isostructurality analysis
XPREP	A command for space group determination
XS	A command for structure solution

KAJIAN PERALIHAN FASA BERSANDARKAN SUHU BAGI HABLUR BERBILANG KOMPONEN HEKSAMETILINTETRAMINA DAN ISONIKOTINAMIDA

ABSTRAK

Dalam kajian ini, tiga puluh satu hablur berbilang komponen heksametilintetramina dan isonikotinamida telah berjaya disediakan dan tujuh daripada mereka mengalami peralihan fasa bersandarkan suhu yang dikaji dengan menggunakan analisis pembelauan sinar-X hablur tunggal di bawah pelbagai suhu. Tujuh hablur berbilang komponen ini adalah heksametilintetramina–asid 2-metilbenzoik (1/2) (monoklinik $P2_1/c$ ↔ ortorombik *Pccn*, T_c = 164.5 (5) K), heksametilintetramina–asid benzoik (1/2) (monoklinik *Pn* ↔ ortorombik *Fmm*2, T_c = 257.5 (5) K), heksametilintetramina–asid 4-metilbenzoik (1/2) (monoklinik $P2_1/n$ ↔ ortorombik *Cmcm*, T_c = 265.5 (5) K), heksametilintetramina–asid suksinik (1/1) (monoklinik $P2_1/n$ ↔ monoklinik $P2_1/c$, T_c = 219 (1) K), heksametilintetramina–asid adipik (1/1) (monoklinik $P2_1$ ↔ monoklinik $P2/n$ ↔ ortorombik $Pna2_1$ ↔ ortorombik *Pbcn* ↔ ortorombik *Cmcm*, $T_{c,1}$ = 202 (2) K, $T_{c,2}$ = 249 (2) K, $T_{c,3}$ = 258 (2) K, $T_{c,4}$ = 293 (2) K), isonikotinamida–asid 4-metoksibenzoik (1/1) (monoklinik $I2/a$ ↔ monoklinik $I2/a$, T_c = 142.5 (5) K) dan isonikotinamida–asid malonik (2/1) (triklinik $P\bar{1}$ ↔ monoklinik $C2/c$, T_c = 295 (1) K). Kajian kristalografi bukan ambien ini telah dijalankan untuk mengkaji perubahan struktur hablur berbilang komponen antara fasa yang berlainan dari 100 hingga 300 K. Peralihan fasa struktur bagi heksametilintetramina–asid 2-metilbenzoik (1/2), heksametilintetramina–asid benzoik (1/2), heksametilintetramina–asid 4-metilbenzoik (1/2), heksametilintetramina–asid suksinik (1/1) dan heksametilintetramina–asid adipik

(1/1) adalah berkaitan dengan transformasi tertib-taktertib struktur sebagai fungsi suhu di dalam struktur hablur. Peralihan fasa struktur bagi isonikotinamida–asid 4-metoksibenzoik (1/1) adalah berkaitan dengan sesaran susunan molekul yang terikat dengan hidrogen dari satah planar. Peralihan fasa struktur yang diperhatikan bagi isonikotinamida–asid malonik (2/1) adalah berkaitan dengan sesaran molekul isonikotinamida dan transformasi konformasi *syn-anti* molekul asid malonik. Peralihan fasa tertib pertama boleh berbalik yang diperhatikan telah disahkan dengan ketajaman puncak-puncak endotermik dan eksotermik daripada pengukuran kalorimetri imbasan pembezaan. Tenaga interaksi antara molekul untuk pasangan molekul yang terpilih dikira dengan kaedah semiempirik *PIXEL* sebagai tambahan kepada analisis lazim ikatan hidrogen antara molekul berdasarkan geometri.

TEMPERATURE-DEPENDENT PHASE TRANSITION STUDIES OF MULTI-COMPONENT CRYSTALS OF HEXAMETHYLENETETRAMINE AND ISONICOTINAMIDE

ABSTRACT

In this research, thirty-one multi-component crystals of hexamethylenetetramine and isonicotinamide were successfully prepared and seven of them undergo temperature-dependent phase transitions, which were investigated by using variable-temperature single-crystal X-ray diffraction analysis. These seven multi-component crystals are hexamethylenetetramine–2-methylbenzoic acid (1/2) (monoclinic $P2_1/c$ ↔ orthorhombic $Pccn$, T_c = 164.5 (5) K), hexamethylenetetramine–benzoic acid (1/2) (monoclinic Pn ↔ orthorhombic $Fmm2$, T_c = 257.5 (5) K), hexamethylenetetramine–4-methylbenzoic acid (1/2) (monoclinic $P2_1/n$ ↔ orthorhombic $Cmcm$, T_c = 265.5 (5) K), hexamethylenetetramine–succinic acid (1/1) (monoclinic $P2_1/n$ ↔ monoclinic $P2_1/c$, T_c = 219 (1) K), hexamethylenetetramine–adipic acid (1/1) (monoclinic $P2_1$ ↔ monoclinic $P2/n$ ↔ orthorhombic $Pna2_1$ ↔ orthorhombic $Pbcn$ ↔ orthorhombic $Cmcm$, $T_{c,1}$ = 202 (2) K, $T_{c,2}$ = 249 (2) K, $T_{c,3}$ = 258 (2) K, $T_{c,4}$ = 293 (2) K), isonicotinamide–4-methoxybenzoic acid (1/1) (monoclinic $I2/a$ ↔ monoclinic $I2/a$, T_c = 142.5 (5) K) and isonicotinamide–malonic acid (2/1) (triclinic $P\bar{1}$ ↔ monoclinic $C2/c$, T_c = 295 (1) K). These non-ambient crystallography studies were carried out to study the structural changes of multi-component crystals between different phases from 100 to 300 K. The structural phase transitions of hexamethylenetetramine–2-methylbenzoic acid (1/2), hexamethylenetetramine–benzoic acid (1/2), hexamethylenetetramine–4-methylbenzoic acid (1/2), hexamethylenetetramine–succinic acid (1/1) and

hexamethylenetetramine–adipic acid (1/1) are associated with the structural order-disorder transformations as a function of temperature in their crystal structures. The structural phase transition of isonicotinamide–4-methoxybenzoic acid (1/1) is associated with the molecular displacements of hydrogen-bonded arrays from planarity. The observed structural phase transition of isonicotinamide–malonic acid (2/1) is associated with the molecular displacement of isonicotinamide molecule and the *syn-anti* conformational transformation of malonic acid molecule. The observed reversible first-order phase transitions were confirmed by the sharp endothermic and exothermic peaks of the differential scanning calorimetry measurement. The intermolecular interaction energies of selected molecular pairs were calculated by semi-empirical *PIXEL* method in addition to the conventional geometry-based intermolecular hydrogen-bond analysis.

CHAPTER 1

INTRODUCTION

1.1 Hexamethylenetetramine

Hexamethylenetetramine ($C_6H_{12}N_4$, IUPAC name: 1,3,5,7-tetraazatricyclo[3.3.1.1^{3,7}]decane and also known as hexamine or urotropine) is a cage-like molecule similar to adamantane but with its tertiary carbon atoms replaced with nitrogen atoms (Figure 1.1). Hexamethylenetetramine is the first solved X-ray crystal structure of an organic compound in 1923 (Dickinson & Raymond, 1923). It is monomorphic and crystallized in a non-centrosymmetric cubic crystal structure (space group $I\bar{4}3m$, a = 7.021 Å) (Becka & Cruickshank, 1963), which does not exhibit any temperature-dependent structural phase transition from 5 to 350 K in heat capacity measurements (Chang & Westrum, 1960). It is highly soluble in water (850 g L^{-1} at 25 °C) and insoluble in diethyl ether (Springsteen, 2014). There are no reports of the acute toxicity of ingested or inhaled hexamethylenetetramine in man, however it still can cause irritation of skin and dermatitis ("Hexamethylenetetramine [MAK Value Documentation, 1993]," 2012).

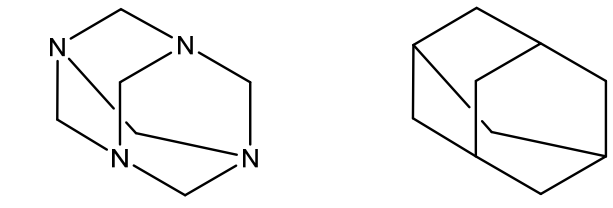

hexamethylenetetramine adamantane

Figure 1.1 Schematic diagrams of hexamethylenetetramine and adamantane.

1.2 Isonicotinamide

Isonicotinamide consists of five polymorphic forms (Aakeröy *et al*., 2003; Eccles *et al*., 2011; Li *et al.*, 2011), which are crystallized in the monoclinic and orthorhombic crystal systems, and it is a good co-crystallizing agent due to its considerable synthon flexibility (Aakeröy *et al*., 2003) in addition to the structural flexibility (Figure 1.2). The pyridine N atom of isonicotinamide is a good hydrogen-bond acceptor, which forms strong interaction with good hydrogen-bond donors such as carboxylic acids and alcohols (Báthori *et al.*, 2011). Nicotinamide, an isomer of isonicotinamide, is classified as a Generally Recognized As Safe (GRAS) substance by the U. S. Food and Drug Administration (FDA) and it makes up with nicotinic acid to form vitamin B_3 complex (Báthori *et al.*, 2011) (Figure 1.2).

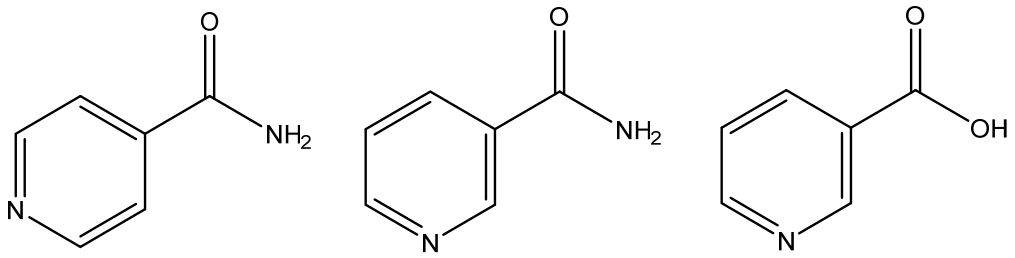

Figure 1.2 Schematic diagrams of isonicotinamide, nicotinamide and nicotinic acid.

1.3 Multi-Component Crystals

Multi-component crystals are increasingly important in improving the physicochemical properties of active pharmaceutical ingredients (API) by co-crystallizing with easy-tuned co-formers (Almarsson & Zaworotko, 2004; Báthori *et al*., 2011; Sowa *et al.*, 2013). Multi-component crystals can be classified into three main classes (solvate, salt and co-crystal) and seven subclasses (true solvate, true salt,

true co-crystal, salt solvate, co-crystal solvate, co-crystal salt and co-crystal salt solvate) under the proposal of Grothe *et al*. (2016) (Figure 1.3). The ΔpK_a rule has been used to predict the formation of multi-component crystal as a neutral co-crystal (ΔpK_a is smaller than 0) or an ionic salt (ΔpK_a is larger than 4) (Bhogala *et al*., 2005; Cruz-Cabeza, 2012; Lemmerer *et al*., 2015). It is noteworthy that the ΔpK_a rule is not absolute within the salt-cocrystal continuum formed in between these two limits.

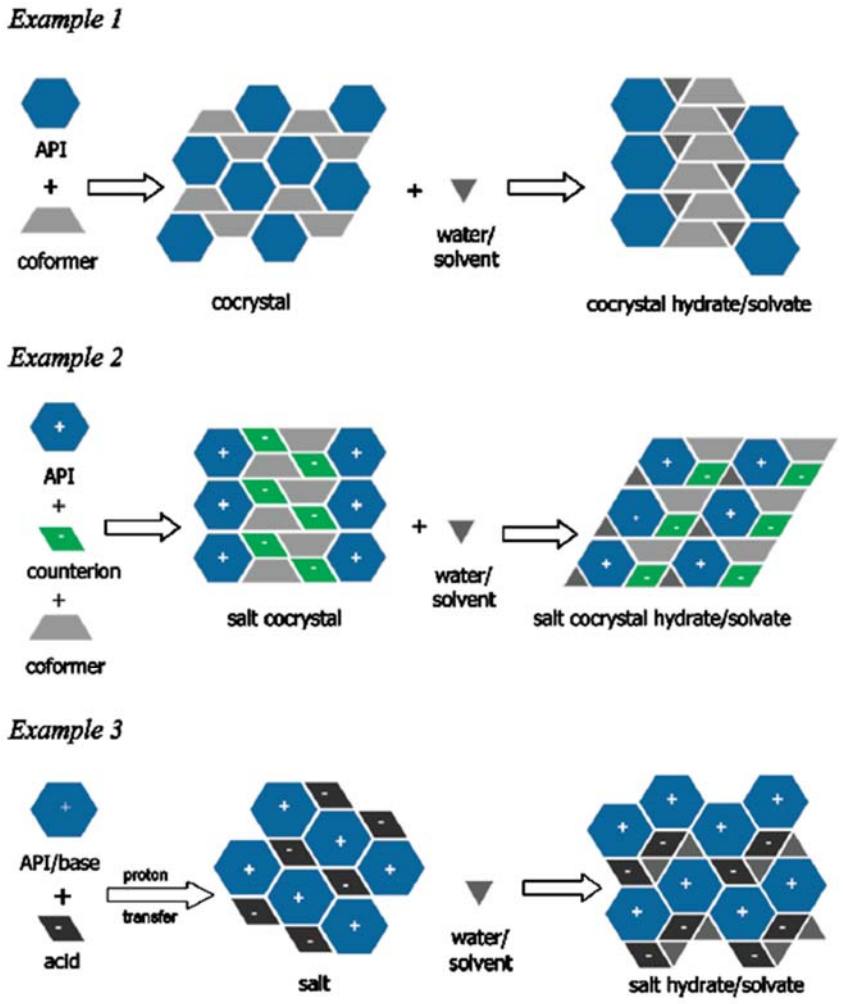

Figure 1.3 The possible multi-component crystals of active pharmaceutical ingredients (API) (Schultheiss & Newman, 2009).

The multi-component crystals of hexamethylenetetramine and alkanedioic acids in 1:1 stoichiometry (HMTA·C*n*, where *n* is the numbers of carbons of alkanedioic acid) are formed as layered structures with alternating sheets of hexamethylenetetramine and alkanedioic acid. The common packing mode of HMTA·C*n* is a one-dimensional *zig-zag* chain, which is similarly observed in other reported hexamethylenetetramine complexes when bifunctional donor molecules are involved (Lemmerer, 2011*a*).

The multi-component crystals of isonicotinamide and carboxylic acids produce well-defined supermolecules with a very consistent pattern of hydrogen-bond preferences (Aakeröy *et al*. 2002), which are heteromeric carboxyl···pyridine and self-complementary carboxamide···carboxamide hydrogen-bonds, taking the advantage of relative positions of carboxamide group and heterocyclic N atom at 1,4-position of the pyridine ring. Five isonicotinamide-alkanedioic acid (2/1) adducts (2IN·C*n*, *n* = 2, 3, 4, 5 and 6, where *n* is the numbers of carbons of alkanedioic acid) were reported to date (Aakeröy *et al.*, 2002; Schmidtmann *et al*., 2007, 2009; Vishweshwar *et al*., 2003*a*). For those adducts with even numbers of *n*, they were crystallized in the monoclinic space group $C2/c$ or the triclinic space group $P\bar{1}$, and consist of a half-molecule of alkanedioic acid and an isonicotinamide molecule in their respective asymmetric unit. The complete alkanedioic acids are generated by a twofold rotational axis or an inversion center in the crystal structures. The monotropic polymorphs of isonicotinamide-oxalic acid (2/1) adduct originated from different conformers (*cis* and *trans*) of oxalic acid were studied (Schmidtmann *et al*., 2007, 2009). The large number of formula units per asymmetric unit ($Z' = 3$) of isonicotinamide-oxalic acid (2/1) adduct reported by Vishweshwar *et al*. (2003*a*) triggered our suspicion of the

possibility of structural phase transition and the high-temperature phase of this adduct was firstly reported in this study.

1.4 Structural Phase Transitions

Polymorphs are multiple crystal forms of a given compound and are categorized as either monotropic or enantiotropic, in which the higher melting form is or isn't thermodynamically stable at all temperatures below the melting point (Carlton, 2011). The enantiotropic polymorphs undergo phase transitions which can be categorized using Ehrenfest's (1933) and Buerger's (1951, 1961, 1972) classifications according to their thermodynamic and structural aspects, respectively. First-order phase transitions exhibit abrupt jumps in their thermodynamic quantities (*e.g.*, internal energy, entropy, enthalpy, *etc.*) and physical properties (*e.g.*, crystal structure). Second-order phase transitions show continuous changes in the thermodynamic quantities, in which the first derivatives are discontinuous. The temperature- or pressure-induced phase transitions can be divided into several types such as displacive (Rybarczyk-Pirek *et al*., 2014; Zhang *et al*., 2013*b*), order-disorder (Brandel *et al*., 2015; Suzuki *et al*., 2014; Wu & Jin, 2013) and reconstructive (Johnston *et al*., 2014; Maloney *et al*., 2014) based on the structural changes. The high-temperature phase of an enantiotropic phase transition of a crystal is commonly higher symmetric than its low-temperature phase; however, isosymmetric transition with same space group symmetry at both phases does exist (Ellena *et al*., 2014; Quah *et al.*, 2012; Swainson *et al.*, 2002; Ye *et al.*, 2010). According to International Union of Crystallography (IUCr), isostructural crystals are two crystals with same structure but not necessarily to have the same cell dimensions nor the same chemical composition, and with a 'comparable' variability in the atomic coordinates to that of the cell dimensions and

chemical composition ("IUCr," 2017). One- and two-dimensional isostructuralities of monotropic polymorphs and three-dimensional isostructurality of enantiotropic polymorphs have been reported and systematically analyzed by visual comparison or automated *XPac* calculation (Coles *et al.*, 2014; Fábián & Kálmán, 1999). Some examples of three-dimensional isostructural crystals, which exhibited structural phase transition(s) at similar transition temperature(s), are Cl/Br exchanged 4-chloro- and 4-bromobenzyl alcohols (Hashimoto & Harada, 2003), N/O exchanged triferrocenylboroxine and triferrocenylborazine (Bats *et al*., 2002), pyridazine fluoroborate and pyridazine perchlorate (Czapla *et al*., 2011), guanidinium iodoantimonate (III) and guanidinium iodobismuthate (III) (Szklarz *et al*., 2008), and phosphonium chloroantimonate (III) and phosphonium chlorobismuthate (III) (Wojtaś & Jakubas, 2004).

m-Carboxyphenylammonium monohydrogenphosphite (Bendeif *et al*., 2005, 2009) is a phosphite salt, which exhibits first-order displacive-type isosymmetric structural phase transition (monoclinic $P2_1/c$ ↔ monoclinic $P2_1/c$) at 246 (2) K, induced by rotation and translation of both cations and anions in the crystal, leading to competition between intra- and intermolecular interactions. The word "displacive" in solid-solid phase transition is referred to structural comparison of low- and high-temperature polymorphic forms of a crystal with similar X-ray crystal structures, which seemed to be as a result of deformation of the original structure by molecular displacements without primary bond breaking. The mechanism of displacive phase transition remained arguable and a general molecular theory of "crystal growth from nucleation in crystal defects" was proposed by Mnyukh *et al.* (1975). Another proposed mechanism is the cooperative motion of hydrogen-bonded bilayers through

an intermediate state in the α↔β enantiotropic transition of DL-norleucine (van den Ende *et al*., 2016).

Order-disorder structural phase transition is triggered by molecular conformation flexibility and molecular rearrangement in a crystal structure, and the transition is associated with or without a space group change (Asghar *et al*., 2016; Khan *et al*., 2015; Quah *et al*., 2012). The molecules of positional or conformational disordered crystals at the high-temperature phase are transformed into a stable state with single position or conformation at the low-temperature phase (Suzuki *et al.*, 2014).

The single-crystals of HMTA·C*n* undergo temperature-induced structural phase transitions before their melting points (Bonin *et al.*, 2003; Bussien Gaillard *et al.*, 1996, 1998; Gardon *et al.*, 2001, 2003; Hostettler *et al.*, 1999; Pinheiro *et al.*, 2003). HMTA·C8 and HMTA·C10 exhibit incommensurate modulated phase at room temperature (Bussien Gaillard *et al.*, 1996, 1998), and the latter crystal was reported to undergo a lock-in transition at 291 K into a commensurate modulated phase (Gardon *et al.*, 2001). HMTA·C7, HMTA·C9, and HMTA·C11 undego a ferroelastic phase transition from a disordered structure at the orthorhombic phase into an ordered structure with induced twinning at the monoclinic phase (Bonin *et al.*, 2003; Gardon *et al.*, 2003; Hostettler *et al.*, 1999; Pinheiro *et al.*, 2003).

1.5 Problem Statement

Crystal polymorphism shows significant impact on physicochemical (solubility, dissolution rate, stability, *etc*.) and mechanical properties (hardness, tensile strength, compressibility, *etc.*), which are extremely important in the fields of solid state physics and material sciences (Censi & Di Martino, 2015; Xiong *et al.*, 2017; Zhang *et al.*, 2013*a*). Most importantly, the structural changes in the pharmaceutical ingredients may alter their biochemical effect and dosage form performance (Kobayashi *et al*., 2000; Raza *et al.*, 2014). With the understanding of the structural details behind the structural phase transitions of polymorphs, we can provide knowledge and assistance to enable reliable and robust production in the field of pharmaceutical sciences. The temperature-dependent conformational and structural changes of the enantiotropic crystals (Chantrapromma *et al.*, 2006; Fun *et al.*, 2007; Quah *et al*., 2012) can be three-dimensional structurally characterized by the state-of-the-art single-crystal X-ray diffraction method at non-ambient conditions. Keeping these facts in mind and taking advantage of good crystallizability, the temperature-dependent structural phase transitions of seven newly prepared multi-component crystals of hexamethylenetetramine and isonicotinamide were determined in this research project by using variable-temperature single-crystal X-ray diffraction analysis and differential scanning calorimetry measurement.

1.6 Research Objectives

The objectives of this research are:

i. To prepare the multi-component crystals of hexamethylenetetramine and isonicotinamide with various carboxylic acids.

ii. To determine the characteristic, reversibility and transition temperature of the observed structural phase transitions by differential scanning calorimetry measurement.

iii. To identify the structural deviations between different temperature phases by variable-temperature single-crystal X-ray diffraction analysis.

iv. To study the supramolecular constructs by conventional hydrogen-bond analysis.

v. To calculate the intermolecular interaction energies of molecular contacts by semi-empirical *PIXEL* method.

CHAPTER 2

THEORY

2.1 Crystalline Material

Three-dimensional crystals are categorized into 7 crystal systems, 14 Bravais lattices, 32 crystal classes (crystallographic point groups) and 230 space groups (Table 2.1). The crystal systems are combined with the centering translations (face centered *F*, body centered *I*, and base centered *A*, *B* and *C*) to reach Bravais lattices. Lattice defines the translational symmetry, whereby point group describes the non-translational symmetry of a crystal. The holohedral point group corresponds to the lattice symmetry, *i.e.*, $\bar{1}$ for triclinic, 2/*m* for monoclinic, *mmm* for orthorhombic, $\bar{3}m$ for rhombohedral, 4/*mmm* for tetragonal, 6/*mmm* for hexagonal and $m\bar{3}m$ for cubic crystal systems. The remaining point groups are merohedral point groups, which are the subgroups of corresponding holohedral point groups in the same crystal systems. The short and full Hermann-Mauguin notations of monoclinic space groups and those space groups with point groups *mmm*, 4/*mmm*, $\bar{3}m$, 6/*mmm*, $m\bar{3}$ and $m\bar{3}m$ are different (Wondratschek & Müller, 2004). The symmetry axes are removed from the former notation as many as possible. For example, the full *vs*. short Hermann-Mauguin notations are $P12_1/c1$ *vs*. $P2_1/c$ for space group no. 14 and $C2/m2/c2_1/m$ *vs*. *Cmcm* for space group no. 63.

Table 2.1 Crystal systems, Bravais lattices and crystallographic point groups of three-dimensional crystals (Giacovazzo *et al.*, 2011; Massa, 2004).

Crystal system	Bravais lattice	Unit-cell parameters	Crystallographic point group* in short Hermann–Mauguin notation	No. of space groups
Triclinic	*P*	$a \neq b \neq c$, $\alpha \neq \beta \neq \gamma$	**1**, $\bar{1}$	2
Monoclinic	*P*, *C* (or *A* or *I*)	$a \neq b \neq c$, $\alpha = \gamma = 90°, \beta > 90°$	**2**, ***m***, 2/*m*	13
Orthorhombic	*P*, *C* (or *A* or *B*), *I*, *F*	$a \neq b \neq c$, $\alpha = \beta = \gamma = 90°$	222, ***mm2***, *mmm*	59
Tetragonal	*P*, *I*	$a = b \neq c$, $\alpha = \beta = \gamma = 90°$	**4**, $\bar{4}$, 4/*m*, 422, **4*mm***, $\bar{4}2m$, 4/*mmm*	68
Trigonal	*P*	$a = b \neq c$, $\alpha = \beta = 90°, \gamma = 120°$ (hexagonal axes)	**3**, $\bar{3}$, 32, ***3m***, $\bar{3}m$	18
	R	$a = b = c$, $\alpha = \beta = \gamma \neq 90°$ (rhombohedral axes)		7
Hexagonal	*P*	$a = b \neq c$, $\alpha = \beta = 90°, \gamma = 120°$	**6**, $\bar{6}$, 6/*m*, 622, ***6mm***, $\bar{6}2m$, 6/*mmm*	27
Cubic	*P*, *I*, *F*	$a = b = c$, $\alpha = \beta = \gamma = 90°$	23, $m\bar{3}$, 432, $\bar{4}3m$, $m\bar{3}m$	36

*Ten polar crystallographic point groups are highlighted as bold.

2.2 Single-Crystal X-ray Crystallography

X-ray crystallography is a generally known field that utilized X-ray diffraction method to determine the three-dimensional crystal structures of target compounds from small molecules to macromolecules at their atomic levels. A single-crystal with long range periodic arrangement of atoms is indispensable for single-crystal X-ray diffraction technique, governing by the principle of diffraction or Bragg's law (equation 2.1, Figure 2.1), to provide sharp diffraction patterns.

$$n\lambda = 2dsin\theta \tag{2.1}$$

where n is the order of reflection, λ is the wavelength of incident beam, d is the interplanar spacing and θ is the incident angle.

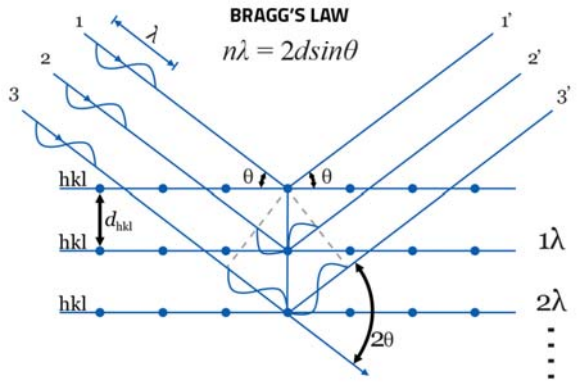

Figure 2.1 Bragg's law ("X-ray diffraction," 2018).

2.2.1 Resultant Wave of *N* Waves

The resultant wave of two scattered waves from two atoms with phase shifts, φ_1 and φ_2, can be represented in the complex form, where

$$\boldsymbol{F} = \boldsymbol{f_1} + \boldsymbol{f_2} = f_1 e^{i\varphi_1} + f_2 e^{i\varphi_2} \tag{2.2}$$

The resultant wave of N waves (Figure 2.2) can then be summarized as

$$\boldsymbol{F} = \sum_{j=1}^{N} f_j e^{i\varphi_j} = \sum_{j=1}^{N} f_j\left(\cos\varphi_j + i\sin\varphi_j\right) = |\boldsymbol{F}|e^{i\varphi} \tag{2.3}$$

The amplitude of $\boldsymbol{F}$ can be calculated by multiplied $\boldsymbol{F}$ with its conjugate $\boldsymbol{F}^*$.

$$|\boldsymbol{F}|^2 = \boldsymbol{F}\boldsymbol{F}^* = |\boldsymbol{F}|e^{i\varphi}|\boldsymbol{F}|e^{-i\varphi} = |\boldsymbol{F}|^2[(\cos\varphi + i\sin\varphi)(\cos\varphi - i\sin\varphi)] \tag{2.4}$$

$$|\boldsymbol{F}| = (|\boldsymbol{F}|^2\cos^2\varphi + |\boldsymbol{F}|^2\sin^2\varphi)^{1/2} \tag{2.5}$$

$$|\boldsymbol{F}| = \left[\left(\sum_{j=1}^{N} f_j \cos\varphi_j\right)^2 + \left(\sum_{j=1}^{N} f_j \sin\varphi_j\right)^2\right]^{1/2} \tag{2.6}$$

Equation (2.6) can be simplified into

$$|\boldsymbol{F}| = \left(A^2 + B^2\right)^{1/2} \tag{2.7}$$

The phase angle φ of resultant wave is then given as

$$\varphi = \tan^{-1} B/A \tag{2.8}$$

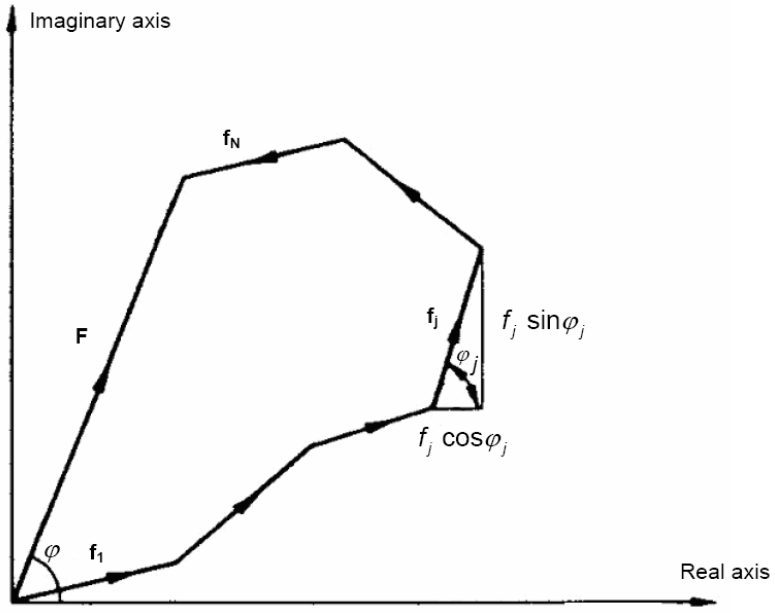

Figure 2.2 The combination of *N* waves (Ladd & Palmer, 1993).

2.2.2 Structure Factor

The phase difference φ of a scattered wave by atom j with partial coordinates (x, y, z) relative to the origin of unit-cell is given as

$$\varphi_j = 2\pi\left(hx_j + ky_j + lz_j\right) \tag{2.9}$$

The structure factor $\boldsymbol{F}_{hkl}$ can be expressed into equation (2.10) using equation (2.9) and some modifications to the equation (2.3).

$$\boldsymbol{F}_{hkl} = \sum_{j=1}^{N} g_j e^{2\pi i\left(hx_j + ky_j + lz_j\right)} \tag{2.10}$$

where g_j is the temperature-corrected atomic scattering factor (Figure 2.3). The structure factor $\boldsymbol{F}_{000}$ at zero scattering angle is equals to the total number of electrons in a unit-cell.

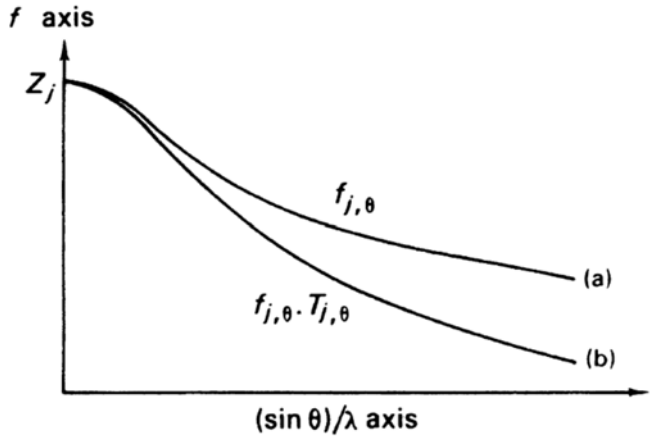

Figure 2.3 Atomic scattering factors. (a) Stationary atom, $f_{j,\theta}$. (b) Atom corrected for thermal vibration, $f_{j,\theta}\ T_{j,\theta}$, also called $g_{j,\theta}$, where $T_{j,\theta} = \exp(-B^2\sin^2\theta/\lambda^2)$ and B is the mean isotropic temperature factor (Ladd & Palmer, 1993).

The intensity of a reflection from a *hkl* plane is proportional to the square of the amplitude of its structure factor (equation 2.11). The reflection data file obtained after the process of data collection, integration and reduction consists of six columns, which comprised of the Miller indices *h*, *k* and *l*, F^2, $\sigma(F^2)$ and batch number, and ends with six zeros at the last row. The standard deviation σ is determined by the data reduction program.

$$I_{hkl} \propto |\boldsymbol{F}_{hkl}|^2 \tag{2.11}$$

2.2.3 Systematic Absences

The non-primitive lattice types and translational symmetry operations (screw axis and glide plane) of a crystal can be identified by the systematic absences of a diffraction pattern.

2.2.3(a) General Absences

By taking a face-centered lattice as an example, the atoms at positions (x_j, y_j, z_j), (x_j, y_j+1/2, z_j+1/2), (x_j+1/2, y_j, z_j+1/2) and (x_j+1/2, y_j+1/2, z_j) are symmetry-equivalent. The structure factor of *N*/4 atoms which are translational related to the rest is expressed as

$$\begin{aligned}\boldsymbol{F}_{hkl} &= \sum_{j=1}^{N/4} g_j \left\{ e^{2\pi i\left(hx_j+ky_j+lz_j\right)} + e^{2\pi i\left(hx_j+ky_j+lz_j+\frac{k}{2}+\frac{l}{2}\right)} \right. \\ &\qquad \left. + e^{2\pi i\left(hx_j+ky_j+lz_j+\frac{h}{2}+\frac{l}{2}\right)} + e^{2\pi i\left(hx_j+ky_j+lz_j+\frac{h}{2}+\frac{k}{2}\right)} \right\} \\ &= \left\{1 + e^{\pi i(k+l)} + e^{\pi i(h+l)} + e^{\pi i(h+k)}\right\} \sum_{j=1}^{N/4} g_j e^{2\pi i\left(hx_j+ky_j+lz_j\right)}\end{aligned} \tag{2.12}$$

$$= \{1 + (-1)^{k+l} + (-1)^{h+l} + (-1)^{h+k}\} \sum_{j=1}^{N/4} g_j e^{2\pi i(hx_j+ky_j+lz_j)}$$

The prefactor $\{1 + (-1)^{k+l} + (-1)^{h+l} + (-1)^{h+k}\}$ and $\boldsymbol{F}_{hkl}$ equal to zero for all (*hkl*) except for those indices with all odd or all even components, which make the prefactor equals to four. The examples of systematic absences of a face-centred lattice are reflections (200), (300), (124) and (136). Similar derivations can be applied to the lattice types *A*, *B*, *C* and *I* with some modifications to the symmetry-equivalent positions. The conditions for general absences of non-primitive lattice types *A*, *B*, *C*, *F* and *I* are presented in Table 2.2.

Table 2.2 Conditions for general absences of non-primitive lattice types *A*, *B*, *C*, *F* and *I* (Massa, 2004).

Lattice types	Reflections affected	Conditions for general absences
P	*hkl*	None
A	*hkl*	$k + l = 2n + 1$
B	*hkl*	$h + l = 2n + 1$
C	*hkl*	$h + k = 2n + 1$
F	*hkl*	*h*, *k*, *l* neither all even nor all odd
I	*hkl*	$h + k + l = 2n + 1$

2.2.3(b) Zonal and Row Absences

Taking the example of a crystal with a *n*-glide perpendicular to the *c*-axis, the equivalent position of an atom *j* at (*x*, *y*, *z*) is (*x*+1/2, *y*+1/2, –*z*). The structure factor can be expressed as

$$\boldsymbol{F}_{hkl} = \sum_{j=1}^{N/2} g_j \left\{ e^{2\pi i(hx_j+ky_j+lz_j)} + e^{2\pi i\left(hx_j+ky_j-lz_j+\frac{h}{2}+\frac{k}{2}\right)} \right\} \qquad (2.13)$$

Equation (2.13) can be simplified to equation (2.14) if we only consider the reflections (*hk*0).

$$\begin{aligned} \boldsymbol{F}_{hk0} &= \sum_{j=1}^{N/2} g_j \left\{ e^{2\pi i(hx_j+ky_j)} + e^{2\pi i\left(hx_j+ky_j+\frac{h}{2}+\frac{k}{2}\right)} \right\} \\ &= \left\{1 + e^{\pi i(h+k)}\right\} \sum_{j=1}^{N/2} g_j e^{2\pi i(hx_j+ky_j)} \\ &= \{1 + (-1)^{h+k}\} \sum_{j=1}^{N/2} g_j e^{2\pi i(hx_j+ky_j)} \end{aligned} \tag{2.14}$$

$\boldsymbol{F}_{hk0}$ equals to zero if $h + k$ is odd and thus, *e.g.* reflections (100), (120), (230) and (300) should be absent in the diffraction pattern. The conditions for zonal and row absences, which only affect the reciprocal lattice planes and lines, respectively, are presented in Tables 2.3 and 2.4.

Table 2.3 Conditions for zonal absences of *a*-, *b*-, *c*- and *n*-glide planes (Massa, 2004).

Glide planes	Orientations	Reflections affected	Conditions for zonal absences
a	⊥*b*	*h*0*l*	$h = 2n + 1$
a	⊥*c*	*hk*0	$h = 2n + 1$
b	⊥*a*	0*kl*	$k = 2n + 1$
b	⊥*c*	*hk*0	$k = 2n + 1$
c	⊥*a*	0*kl*	$l = 2n + 1$
c	⊥*b*	*h*0*l*	$l = 2n + 1$
n	⊥*a*	0*kl*	$k + l = 2n + 1$
n	⊥*b*	*h*0*l*	$h + l = 2n + 1$
n	⊥*c*	*hk*0	$h + k = 2n + 1$

Table 2.4 Conditions for row absences of 2_1 screw axis (Massa, 2004).

Screw axis	Orientations	Reflections affected	Conditions for row absences
2_1	∥*a*	*h*00	$h = 2n + 1$
2_1	∥*b*	0*k*0	$k = 2n + 1$
2_1	∥*c*	00*l*	$l = 2n + 1$

2.2.4 Structure Solution

The diffraction data collection measures only the intensities and their standard deviations but not the phase angles of the reflections on a detector. The phase problem of crystallography can be solved by direct methods, which are based on the atomicity, positivity and randomness of the electron density function (Blake *et al.*, 2009; Giacovazzo *et al.*, 2011). The Fourier synthesis of the observed structure factors with their solved phases give the electron density of the crystal structure. The electron density ρ at the fractional coordinate (x, y, z) in a unit-cell of volume V is given as

$$\rho_{xyz} = \frac{1}{V}\sum_{h}\sum_{\substack{k\\-\infty}}^{\infty}\sum_{l}\boldsymbol{F}_{hkl}e^{-2\pi i(hx+ky+lz)} \tag{2.15}$$

and can be simplified into

$$\rho_{xyz} = \frac{1}{V}\sum_{h}\sum_{\substack{k\\-\infty}}^{\infty}\sum_{l}|\boldsymbol{F}_{hkl}|\cos[2\pi(hx+ky+lz)-\varphi_{hkl}] \tag{2.16}$$

since ρ_{xyz} is a real number.

2.2.5 Structure Refinement

The initial phase information obtained from direct methods is incomplete and contains definite errors, and thus structure refinement is important for an accurate structure model. The structure refinements of small molecules are conducted by full-matrix least-squares method to minimize the difference between the observed and calculated structure factors, F_o and F_c. The difference Fourier synthesis is particularly useful to locate the positions of hydrogen atoms in an organic structure (Massa, 2004). The refinements against F^2 and F give $wR(F^2)$ and $R[F^2>2\sigma(F^2)]$ indices, respectively.

$$wR(F^2) = \left\{\frac{\sum\left[w({F_o}^2 - {F_c}^2)^2\right]}{\sum\left[w({F_o}^2)^2\right]}\right\}^{1/2} \tag{2.17}$$

$$R[F^2 > 2\sigma(F^2)] = \frac{\sum\left||F_o| - |F_c|\right|}{\sum|F_o|} \tag{2.18}$$

The goodness of fit, S, of a compelete refinement should be close to unity.

$$S = \left\{\frac{\sum\left[w\left({F_O}^2 - {F_C}^2\right)^2\right]}{(n-p)}\right\}^{1/2} \tag{2.19}$$

where n is the number of independent reflections and p is the number of parameters.

The weighting scheme, w, is defined as

$$w = \frac{1}{\sigma^2\left({F_O}^2\right) + (aP)^2 + bP} \tag{2.20}$$

where P is $[2F_c^2 + \mathrm{Max}(F_o^2,0)] / 3$.

2.3 Crystal Twinning

The twin domains of a twinned crystal are related by a specific symmetry operation, *i.e.*, rotation, reflection or inversion, which can be described as a twin matrix. The reflections from different twin domains may overlap completely or partially and superposed into the diffraction pattern with weighted intensities according to the twin scale factor. The former case (merohedral, pseudo-merohedral or reticular-merohedral twin) with complete overlapping occurs due to the higher symmetry of the point group of a crystal lattice as compared to the point group of its crystal structure. For example, a crystal structure of monoclinic space group $P2_1/c$ with point group $2/m$ may emulate as an orthorhombic lattice with point group *mmm* if the unique angle β is very close to 90°, inducing a pseudo-merohedral twin (Müller *et al.*, 2006; Parsons, 2003). The twin law of the former case is a symmetry operator of the point group of the crystal lattice but not of the point group of its crystal structure and it converts all integral Miller indices into other integral triples. The latter case with partial overlapping is also referred to the non-merohedral twin, in which the twin law does not belong to the symmetry of the point group of the crystal lattice nor of the crystal structure but a higher symmetry supercell. The quantity $|E^2 - 1|$ of the intensity statistic of a twinned crystal structure, where E is the normalized structure factor, may be found in the range of 0.4–0.7 as compared to the ideal centrosymmetric and non-centrosymmetric structures with the values of 0.97 and 0.74, respectively.

Twinned crystals are induced if the low-temperature phase belongs to a *translationengleiche* subgroup of the high-temperature phase of a phase transition such as the monoclinic-to-orthorhombic phase transition observed in barbituric acid dihydrate crystal ($P2_1/n \leftrightarrow Pnma$) (Nichol & Clegg, 2005) and Boc-γ^4(*R*)Val-Val-OH

crystal ($P2_1 \leftrightarrow P22_12_1$) (Pal *et al.*, 2014). However, antiphase domains which do not show up in the X-ray diffraction are formed if the low-temperature phase is a *klassengleiche* subgroup associated with lost translational symmetry (Müller, 2013). The subgroup H is a *translationengleiche* subgroup of space group G if G and H possess the same group of translations (*i.e.*, same lattice type), and thus H belongs to a lower symmetry point group than G (Müller, 2013). However, H is a *klassengleiche* subgroup of G if G and H belong to the same point group, and thus H with an enlarged primitive unit-cell has fewer translations than G (Müller, 2013). A general subgroup is neither *klassengleiche* nor *translationengleiche* (Müller, 2013). In contrast, a maximal subgroup is either a *klassengleiche* or a *translationengleiche* subgroup of a space group if there exists no intermediate group (Müller, 2013).

2.4 Ferroic Classification of Structural Phase Transition

Ferroelectric structural phase transition occurs from a non-polar point group (*e.g.*, 2/*m* and *mmm*) to a polar point group (*e.g.*, 2 and *mm*2) in same crystal system, while ferroelastic transition occurs from a non-polar point group to another non-polar point group of different crystal systems (Tolédano & Tolédano, 1987). The transition with both ferroelectric and ferroelastic properties occurs from a non-polar point group to a polar point group associated with a change of crystal system.

2.5 Differential Scanning Calorimetry Measurement

Differential scanning calorimetry measurement is used to determine the glass transition temperature of amorphous material, the melting and boiling points, the relative stability of monotropic and enantiotropic polymorphs, the changes in heat capacity, *etc*. ("DSC theory," 2017). In general, DSC measurement records the amount of heat released or absorbed associated with exothermic and endothermic reactions, respectively, as a function of temperature. The difference in heat flow, dQ/dt, between the sample and the reference is expressed as

$$\Delta(dQ/dt)_P = (dQ/dt)_{P,sample} - (dQ/dt)_{P,reference} \tag{2.21}$$

The heat flow at constant pressure is equivalent to the enthalpy change and thus

$$\Delta(dH/dt) = (dH/dt)_{sample} - (dH/dt)_{reference} \tag{2.22}$$

$\Delta(dH/dt)$ is positive for an endothermic process and is negative for an exothermic process. The peak area corresponds to the enthalpy change, ΔH, of the sample. Enthalpy and entropy are two important properties of a thermodynamic system. Enthalpy, H, is a measure of the heat content of a system. Entropy, S, is a measure of the dispersed energy within a system at a given temperature.

2.6 Non-Covalent Interaction Energies

The total interaction effects can be separated into four terms: Coulombic, polarization, dispersion and repulsion. Coulombic interaction is important for the ionic bonds and hydrogen-bonds, involving permanent charged groups with opposite signs (+ and –) and partially charged groups with opposite signs (δ+ and δ–), respectively. In a crystal, the coulombic energies are commonly overall stabilizing since there is no orientational freedom, however some intermolecular coulombic energies may also be destabilizing (Gavezzotti, 2007). Polarization represents the effect of an external electric field produced by the distribution of charges of the approaching polarized molecule onto the distribution of charges of the polarized molecule. The polarization energy is always stabilizing as the induced dipole of a polarized molecule always points along the stabilizing direction (Gavezzotti, 2007). Dispersion may represent as the secondary mutual polarization due to the correlation of electronic movements of two interacting molecules, which causes the formation of instantaneous dipoles. The dispersion energy is always stabilizing. Repulsion avoids electrons with same spins getting close to the region of intermolecular contact. The exchange-repulsion energy is overall destabilizing. In this thesis, the intermolecular interaction energies of selected molecular pairs were calculated by semi-empirical *PIXEL* method (Gavezzotti, 2003, 2008), which has been extensively used to provide results comparable to other quantum chemical calculations (*i.e.*, periodic density functional theory, symmetry-adapted perturbation theory and dispersion-corrected density functional theory) (Hathwar *et al*., 2015; Moggach *et al*., 2015; Panini & Chopra, 2013, 2014; Panini *et al*., 2014), in addition to the conventional hydrogen-bond analysis.

CHAPTER 3

METHODOLOGY

3.1 Samples Preparation

All chemicals were purchased and used without further purification. Carboxylic acids and hexamethylenetetramine or isonicotinamide (Figure 3.1) were prepared in 1:1, 1:2 or 2:1 molar ratio and dissolved in methanol while heating on a hot plate. Both solutions were then mixed in drop-wise, stirred evenly and heated until a clear mixture was obtained. The diffraction quality single-crystals of thirty-one multi-component crystals of hexamethylenetetramine and isonicotinamide were formed *via* slow evaporation at ambient conditions. All newly prepared multi-component crystals were subjected to the crystal structure screening through Cambridge Structural Database (CSD, version 5.38 with 3 updates: Nov 2016, Feb 2017 and May 2017) (Groom *et al*., 2016) to check the publication status.

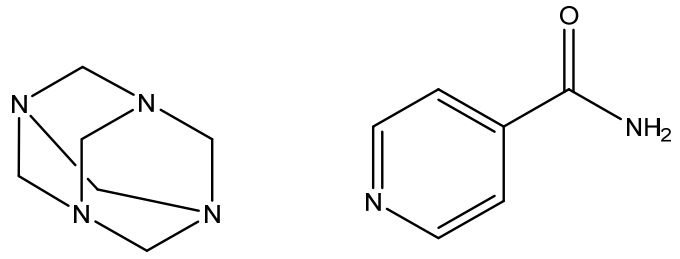

hexamethylenetetramine isonicotinamide

Figure 3.1 Schematic diagrams of hexamethylenetetramine and isonicotinamide.